

This is the final peer-reviewed accepted manuscript of:

A. Armato et al, *A CUPID Li2100MoO4 scintillating bolometer tested in the CROSS underground facility*, 2021 JINST 16 P02037.

The final published version is available online at: <https://doi.org/10.1088/1748-0221/16/02/P02037>

Terms of use:

Some rights reserved. The terms and conditions for the reuse of this version of the manuscript are specified in the publishing policy. For all terms of use and more information see the publisher's website.

This item was downloaded from IRIS Università di Bologna (<https://cris.unibo.it/>)

When citing, please refer to the published version.

2 A CUPID $\text{Li}_2^{100}\text{MoO}_4$ scintillating bolometer tested in the 3 CROSS underground facility

4 A. Armatol,^a E. Armengaud,^a W. Armstrong,^b C. Augier,^c F. T. Avignone III,^d O. Azzolini,^e
5 I. C. Bandac,^f A. S. Barabash,^g G. Bari,^h A. Barresi,^{i,j} D. Baudin,^a F. Bellini,^{k,l} G. Benato,^m
6 M. Beretta,ⁿ L. Bergé,^o Ch. Bourgeois,^o M. Biassoni,ⁱ J. Billard,^c V. Boldrini,^{p,h} A. Branca,^{i,j}
7 C. Brofferio,^{i,j} C. Bucci,^m J. M. Calvo-Mozota,^f J. Camilleri,^q A. Candela,^m S. Capelli,^{i,j}
8 L. Cappelli,^m L. Cardani,^k P. Carniti,^{i,j} N. Casali,^k A. Cazes,^c E. Celi,^{m,r} C. Chang,^b
9 M. Chapellier,^o A. Charrier,^s D. Chiesa,^{i,j} M. Clemenza,^{i,j} I. Colantoni,^{k,t} F. Collamati,^k
10 S. Copello,^{u,v} O. Cremonesi,ⁱ R. J. Creswick,^d A. Cruciani,^k A. D'Addabbo,^{m,r}
11 G. D'Imperio,^k I. Dafinei,^k F. A. Danevich,^w M. de Combarieu,^s M. De Deo,^m M. De Jesus,^c
12 P. de Marcillac,^o S. Dell'Oro,^{i,j} S. Di Domizio,^{u,v} V. Dompe,^{m,r} A. Drobizhev,^x L. Dumoulin,^o
13 G. Fantini,^{k,l} M. Faverzani,^{i,j} E. Ferri,^{i,j} F. Ferri,^a F. Ferroni,^{k,r} E. Figueroa-Feliciano,^y
14 J. Formaggio,^z A. Franceschi,^{aa} C. Fu,^{ab} S. Fu,^{ab} B. K. Fujikawa,^x J. Gascon,^c
15 A. Giachero,^{i,j} L. Gironi,^{i,j} A. Giuliani,^o P. Gorla,^m C. Gotti,ⁱ P. Gras,^a M. Gros,^a E. Guerard,^o
16 T. D. Gutierrez,^{ac} K. Han,^{ad} E. V. Hansen,ⁿ K. M. Heeger,^{ae} D. L. Helis,^a H. Z. Huang,^{ab,af}
17 R. G. Huang,^{n,x} A. Ianni,^m L. Imbert,^o J. Johnston,^z A. Juillard,^c G. Karapetrov,^{ag}
18 G. Keppel,^e H. Khalife,^o V. V. Kobychyev,^w Yu. G. Kolomensky,^{n,x} S. I. Konovalov,^g Y. Liu,^{ah}
19 P. Loaiza,^o L. Ma,^{ab} M. Madhukuttan,^o F. Mancarella,^{p,h} R. Mariam,^o L. Marini,^{n,x,m}
20 S. Marnieros,^o M. Martinez,^{ai,aj} R. H. Maruyama,^{ae} B. Mauri,^a D. Mayer,^z Y. Mei,^x S. Milana,^k
21 D. Misiak,^c T. Napolitano,^{aa} M. Nastasi,^{i,j} X.-F. Navick,^a J. Nikkel,^{ae} R. Nipoti,^{p,h} S. Nisi,^m
22 C. Nones,^a E. B. Norman,^{n,ak} V. Novosad,^b I. Nutini,^{i,j} T. O'Donnell,^q G. Olivier,^o E. Olivieri,^o
23 C. Oriol,^o J. L. Ouellet,^z S. Pagan,^{ae} C. Pagliarone,^m L. Pagnanini,^{m,r} P. Pari,^s
24 L. Pattavina,^{m,1} B. Paul,^a M. Pavan,^{i,j} H. Peng,^{al} G. Pessina,ⁱ V. Pettinacci,^k C. Pira,^e
25 S. Pirro,^m D. V. Poda,^o T. Polakovic,^b O. G. Polischuk,^w S. Pozzi,^{i,j} E. Previtali,^{i,j} A. Puiu,^{m,r}
26 A. Ressa,^{k,l} D. Reynet,^o R. Rizzoli,^{p,h} C. Rosenfeld,^d V. Sanglard,^c J. A. Scarpaci,^o
27 B. Schmidt,^{y,x} V. Sharma,^q V. N. Shlegel,^{am} V. Singh,ⁿ M. Sisti,ⁱ D. Speller,^{an,ae}
28 P. T. Surukuchi,^{ae} L. Taffarello,^{ao} O. Tellier,^a C. Tomei,^k V. I. Tretyak,^w A. Tsymbaliuk,^e
29 M. Velazquez,^{ap} K. J. Vetter,ⁿ S. L. Wagaarachchi,ⁿ G. Wang,^b L. Wang,^{ah} B. Welliver,^x
30 J. Wilson,^d K. Wilson,^d L. A. Winslow,^z M. Xue,^{al} L. Yan,^{ab} J. Yang,^{al} V. Yefremenko,^b
31 V. I. Yumatov,^g M. M. Zarytskyy,^w J. Zhang,^b A. S. Zolotarova,^o S. Zucchelli,^{h,aa}

32 ^aIRFU, CEA, Université Paris-Saclay, F-91191 Gif-sur-Yvette, France

33 ^bArgonne National Laboratory, Argonne, IL 60439, USA

34 ^cUniv Lyon, Université Lyon 1, CNRS/IN2P3, IP2I-Lyon, F-69622, Villeurbanne, France

35 ^dDepartment of Physics and Astronomy, University of South Carolina, Columbia, SC 29208, USA

¹Also at: Physik-Department, Technische Universität München, Garching, Germany

36 ^e INFN – Laboratori Nazionali di Legnaro, Legnaro (Padova) I-35020, Italy
37 ^f Laboratorio Subterráneo de Canfranc, 22880 Canfranc-Estación, Spain
38 ^g National Research Centre Kurchatov Institute, Institute of Theoretical and Experimental Physics, 117218
39 Moscow, Russia
40 ^h INFN – Sezione di Bologna, Bologna I-40127, Italy
41 ⁱ INFN – Sezione di Milano Bicocca, Milano I-20126, Italy
42 ^j Dipartimento di Fisica, Università di Milano-Bicocca, Milano I-20126, Italy
43 ^k INFN – Sezione di Roma, Roma I-00185, Italy
44 ^l Dipartimento di Fisica, Sapienza Università di Roma, Roma I-00185, Italy
45 ^m INFN – Laboratori Nazionali del Gran Sasso, I-67100 Assergi (AQ), Italy
46 ⁿ University of California, Berkeley, CA 94720, USA
47 ^o Université Paris-Saclay, CNRS/IN2P3, IJCLab, 91405 Orsay, France
48 ^p Istituto per la Microelettronica e Microsistemi, Consiglio Nazionale delle Ricerche, 40129, Bologna, Italy
49 ^q Center for Neutrino Physics, Virginia Polytechnic Institute and State University, Blacksburg, Virginia
50 24061, USA
51 ^r INFN – Gran Sasso Science Institute, L'Aquila I-67100, Italy
52 ^s IRAMIS, CEA, Université Paris-Saclay, F-91191 Gif-sur-Yvette, France
53 ^t Istituto di Nanotecnologia, Consiglio Nazionale delle Ricerche, c/o Dip. Fisica, Sapienza Università di
54 Roma, 00185 Roma, Italy
55 ^u INFN – Sezione di Genova, Genova I-16146, Italy
56 ^v Dipartimento di Fisica, Università di Genova, Genova I-16146, Italy
57 ^w Institute for Nuclear Research of NASU, 03028 Kyiv, Ukraine
58 ^x Lawrence Berkeley National Laboratory, Berkeley, CA 94720, USA
59 ^y Department of Physics & Astronomy, Northwestern University, Evanston, IL 60208-3112, USA
60 ^z Massachusetts Institute of Technology, Cambridge, MA 02139, USA
61 ^{aa} INFN – Laboratori Nazionali di Frascati, Frascati (Roma) I-00044, Italy
62 ^{ab} Key Laboratory of Nuclear Physics and Ion-beam Application (MOE), Fudan University, Shanghai 200433,
63 China
64 ^{ac} Physics Department, California Polytechnic State University, San Luis Obispo, CA 93407, USA
65 ^{ad} INPAC and School of Physics and Astronomy, Shanghai Jiao Tong University; Shanghai Laboratory for
66 Particle Physics and Cosmology, Shanghai 200240, China
67 ^{ae} Wright Laboratory, Department of Physics, Yale University, New Haven, CT 06520, USA
68 ^{af} Department of Physics and Astronomy, University of California, Los Angeles, CA 90095, USA
69 ^{ag} Department of Physics, Drexel University, Philadelphia, PA 19104, USA
70 ^{ah} Beijing Normal University, Beijing 100875, China
71 ^{ai} Laboratorio de Física Nuclear y Astroparticulas, Universidad de Zaragoza, 50009 Zaragoza, Spain
72 ^{aj} Fundación Agencia Aragonesa para la Investigación y el Desarrollo, 50018 Zaragoza, Spain
73 ^{ak} Lawrence Livermore National Laboratory, Livermore, CA 94550, USA
74 ^{al} Department of Modern Physics, University of Science and Technology of China, Hefei 230027, China
75 ^{am} Nikolaev Institute of Inorganic Chemistry, 630090 Novosibirsk, Russia
76 ^{an} Johns Hopkins University, Baltimore, MD 21218, USA
77 ^{ao} INFN – Sezione di Padova, Padova I-35131, Italy
78 ^{ap} Université Grenoble Alpes, CNRS, Grenoble INP, SIMAP, 38402 Saint Martin d'Hères, France
79 ^{aq} Dipartimento di Fisica e Astronomia, Alma Mater Studiorum – Università di Bologna, Bologna I-40127,
80 Italy
81 E-mail: cupid.publications@lngs.infn.it, cross.publications@lsc-canfranc.es

82 ABSTRACT: A scintillating bolometer based on a large cubic $\text{Li}_2^{100}\text{MoO}_4$ crystal (45 mm side) and a
83 Ge wafer (scintillation detector) has been operated in the CROSS cryogenic facility at the Canfranc
84 underground laboratory in Spain. The dual-readout detector is a prototype of the technology that
85 will be used in the next-generation $0\nu 2\beta$ experiment CUPID. The measurements were performed
86 at 18 and 12 mK temperature in a pulse tube dilution refrigerator. This setup utilizes the same
87 technology as the CUORE cryostat that will host CUPID and so represents an accurate estimation
88 of the expected performance. The $\text{Li}_2^{100}\text{MoO}_4$ bolometer shows a high energy resolution of 6 keV
89 FWHM at the 2615 keV γ line. The detection of scintillation light for each event triggered by the
90 $\text{Li}_2^{100}\text{MoO}_4$ bolometer allowed for a full separation ($\sim 8\sigma$) between $\gamma(\beta)$ and α events above 2 MeV.
91 The $\text{Li}_2^{100}\text{MoO}_4$ crystal also shows a high internal radiopurity with ^{228}Th and ^{226}Ra activities of
92 less than 3 and 8 $\mu\text{Bq/kg}$, respectively. Taking also into account the advantage of a more compact
93 and massive detector array, which can be made of cubic-shaped crystals (compared to the cylindrical
94 ones), this test demonstrates the great potential of cubic $\text{Li}_2^{100}\text{MoO}_4$ scintillating bolometers for
95 high-sensitivity searches for the ^{100}Mo $0\nu 2\beta$ decay in CROSS and CUPID projects.

96 KEYWORDS: Double-beta decay, Cryogenic detector, Bolometer, Crystal scintillator, Lithium molyb-
97 date, Particle identification, Radiopurity

98 ARXIV EPRINT: [2011.13806](https://arxiv.org/abs/2011.13806)

99	Contents	
100	1 Introduction	1
101	2 Detector construction and operation	4
102	2.1 $\text{Li}_2^{100}\text{MoO}_4$ scintillating bolometer fabrication	4
103	2.2 Low-temperature underground measurements	5
104	3 Results	6
105	3.1 Detector performance	6
106	3.2 Particle identification capability	9
107	3.3 $\text{Li}_2^{100}\text{MoO}_4$ crystal radiopurity	11
108	4 Conclusions	13

109 1 Introduction

110 Neutrinoless double-beta ($0\nu 2\beta$) decay is a unique probe of new physics beyond the Standard Model
 111 [? ?] and the observation of this process, suggested about 80 years ago but not yet detected (in
 112 contrast to two-neutrino double-beta ($2\nu 2\beta$) decay [?]), would conclusively demonstrate lepton
 113 number violation and the Majorana nature of neutrinos (i.e. a particle that is equal to its own
 114 anti-particle).

115 The bolometric technology, which relies on the use of low-temperature calorimeters acting
 116 simultaneously as a 2β source and a detector, is among the few experimental approaches providing
 117 world-leading sensitivity to $0\nu 2\beta$ decay to-date [?]. In addition to high detection efficiency of
 118 the “ 2β source = detector” technique, bolometers offer high energy resolution, scalability to a large
 119 detector mass via arrays of modules, and the possibility to use different and radiopure materials
 120 containing the most promising 2β isotopes (e.g. see [? ? ?]). Additionally, recent technological
 121 advances have demonstrated the ability to do particle identification [? ? ?], allowing for a reduction
 122 of backgrounds in the signal region of interest by multiple orders of magnitude.

123 Bolometric techniques for $0\nu 2\beta$ decay searches have been developed for about 30 years and
 124 have resulted in the first tonne-scale bolometric experiment CUORE (Cryogenic Underground
 125 Observatory of Rare Events) [?]. CUORE has been in operation at the Gran Sasso underground
 126 laboratory (Italy) since 2017, searching for $0\nu 2\beta$ decay of ^{130}Te (Q -value of the 2β transition, $Q_{2\beta}$,
 127 is 2528 keV [?]). In spite of this extraordinary achievement, the CUORE $0\nu 2\beta$ sensitivity is
 128 limited by a background ($\sim 10^{-2}$ counts/yr/kg/keV) coming from alpha decays at surfaces despite
 129 the highly radiopure materials used for the detector construction. This is due to the use of pure
 130 thermal detectors based on tellurium dioxide crystals (TeO_2 ; 34% of ^{130}Te in natural tellurium [?
 131]) which have the same bolometric response irrespective of the type of the particle interaction [?].

132 CUPID (CUORE Upgrade with Particle IDentification) is a proposed next-generation $0\nu 2\beta$
133 bolometric experiment [?], which will reuse the CUORE infrastructure for the operation of a
134 similar-scale isotopically enriched detector with a background $\sim 10^{-4}$ counts/yr/kg/keV in the region
135 of interest, thus probing $0\nu 2\beta$ decay in so-called “zero-background” conditions. The suppression
136 of the alpha-induced background to a negligible level (i.e. 99.9% of alpha events rejection), while
137 keeping almost 100% of the signal efficiency, is required for particle identification technology. The
138 detector performance is expected to be similar to CUORE and predecessors, with a 5 keV FWHM
139 at $Q_{2\beta}$ as a goal. The activities of ^{226}Ra , ^{228}Th , and ^{232}Th in the enriched bolometers are required
140 to be less than $10 \mu\text{Bq/kg}$, making the contribution of the U/Th crystal bulk activity to be below
141 $\sim 10^{-4}$ counts/yr/kg/keV. The total bulk radioactivity of the crystals should not exceed the mBq/kg
142 level to avoid impacting the detector operation and background with pile-ups [? ? ? ?].

143 Four isotopes, ^{82}Se ($Q_{2\beta} = 2998$ keV [?]), ^{100}Mo (3034 keV [?]), ^{116}Cd (2813 keV [?]) and
144 ^{130}Te , were considered in the CUPID R&D program [?] as isotopes of interest to be embedded in
145 the CUPID detector for the following reasons:

- 146 • The $0\nu 2\beta$ decay energy of these isotopes (except for ^{130}Te) is greater than 2.6 MeV, the
147 end-point of the most energetic intense natural γ -ray radiation;
- 148 • Enrichment is available at a large amount and reasonable cost;
- 149 • Compounds containing these isotopes can be grown into single crystals usable for cryogenic
150 applications;
- 151 • Some of Se-, Mo-, or Cd-containing crystals are also reasonably efficient low-temperature
152 scintillators. The detection of scintillation light using an auxiliary optical bolometer in
153 coincidences with the measurement of particle-induced energy release in the scintillating
154 absorber is a viable tool for particle identification. This technique can also be applied for
155 poorly or non-scintillating crystals, as TeO_2 , to detect Cherenkov radiation allowing particle
156 identification (however, more performing light detectors are demanded to detect a tiny signal).

157 Efficient alpha background rejection has been demonstrated with detectors containing each of these
158 isotopes [? ? ? ? ?]. This paves the way for a future study of $0\nu 2\beta$ across multiple isotopes [?]
159 in case a discovery is made. Based on performance and cost, CUPID selected ^{100}Mo embedded in
160 lithium molybdate (Li_2MoO_4) scintillating crystals [?].

161 The technology of ^{100}Mo -enriched lithium molybdate ($\text{Li}_2^{100}\text{MoO}_4$) scintillating bolometers
162 has been recently developed within the LUMINEU project and it provides [? ?]:

- 163 • A know-how for the mass production of high-quality large radiopure crystals with only few
164 % losses of the enriched material;
- 165 • The fabrication of a detector module (which can be easily mount into array) with energy
166 resolution comparable to that of TeO_2 bolometers, but with a significantly higher α rejection
167 efficiency (e.g. see in [?]).

168 Excellent performances of $\text{Li}_2^{100}\text{MoO}_4$ scintillating bolometers based on cylindrical crystals ($\varnothing 44 \times 45$
169 mm, ~ 0.21 kg, $\sim 97\%$ enrichment in ^{100}Mo) have been demonstrated in single-module and 4-crystal-
170 array tests of LUMINEU [? ? ?] at the Gran Sasso and Modane (LSM; France) underground

171 laboratories. These results have been recently confirmed by the CUPID-Mo experiment [? ? ?] on
172 the scale of a 20-detector array operated at the LSM. Furthermore, the crystal production protocol,
173 adopted by LUMINEU and CUPID-Mo, has been used for the fabrication of 32 $\text{Li}_2^{100}\text{MoO}_4$ crystals
174 0.28 kg each (the average enrichment in ^{100}Mo is 97.7(3)%) for the CROSS (Cryogenic Rare-event
175 Observatory with Surface Sensitivity) $0\nu 2\beta$ experiment [?].

176 CROSS, considered as a part of CUPID R&D, is a project aiming at the development of
177 $\text{Li}_2^{100}\text{MoO}_4$ and $^{130}\text{TeO}_2$ surface-coated bolometers capable of identifying a near surface particle
178 interaction via pulse-shape analysis [?]. A key ingredient of the CROSS technology is crystal-
179 surface coating with a superconducting material to modify the signal pulse-shape for an event
180 occurring at its proximity. The CROSS detector performance and radiopurity should be in compli-
181 ance with CUPID requirements. The feasibility of a highly-efficient identification of near-surface
182 α interactions has recently been demonstrated in multiple tests of the CROSS prototypes [? ? ?
183 ?]. A final validation of the technology is planned to be realized as a $0\nu 2\beta$ experiment with at
184 least 32 $\text{Li}_2^{100}\text{MoO}_4$ bolometers (the addition of the 20 crystals from CUPID-Mo are now also in
185 consideration), hosted in a dedicated cryostat at the Canfranc underground laboratory (Spain). The
186 sensitivity of this medium-scale demonstrator [?] is expected to be on the level of the leading
187 $0\nu 2\beta$ experiments, which have masses larger by a factor 10–100.

188 In contrast to LUMINEU and CUPID-Mo, CROSS is going to use cubic $\text{Li}_2^{100}\text{MoO}_4$ elements
189 with a 45 mm side. The choice of a cubic shape is driven by the possibility to realize a more
190 compact array structure, which allows to deploy a $\sim 30\%$ higher isotope mass in the available
191 experimental volume, and yields an enhanced efficiency in rejecting background-like events that
192 release energy in neighboring crystals (coincidences). Indeed, a volume (i.e. mass) of a cylindrical
193 crystal with a diameter and height equal to the side of the cubic one is almost 30% less (similar
194 to CUPID-Mo vs. CROSS crystals). It is also evident that the efficiency of coincidences between
195 larger, particularly neighbor, detectors would be increased too. The CROSS development of an array
196 of cubic $\text{Li}_2^{100}\text{MoO}_4$ bolometers is also an important benchmark for the design of the final CUPID
197 structure, initially considered to be based on cylindrical ($\varnothing 50 \times 50$ mm) $\text{Li}_2^{100}\text{MoO}_4$ scintillating
198 bolometers [?]. Before using the crystals in the CROSS and CUPID $0\nu 2\beta$ experiments, it is
199 necessary to perform low-temperature test(s) to demonstrate that:

- 200 • Bolometric and spectrometric performances of cubic-shaped $\text{Li}_2^{100}\text{MoO}_4$ scintillating bolome-
201 ters, operated in modern pulse-tube cryostats with possible vibration disturbances, are similar
202 to those of cylindrical $\text{Li}_2^{100}\text{MoO}_4$ detectors tested in dry and/or wet dilution refrigerators;
- 203 • Scintillation light yield of the cubic-shaped and cylindrical crystals is similar, thus providing
204 a highly efficient particle identification;
- 205 • Radioactive contamination of cubic $\text{Li}_2^{100}\text{MoO}_4$ crystals is compatible to that of cylindrical
206 ones.

207 With these goals in mind, we realized a first investigation of a scintillating bolometer based on a
208 large-volume ($\sim 90 \text{ cm}^3$) cubic-shaped $\text{Li}_2^{100}\text{MoO}_4$ crystal, described in the present paper. This
209 study is undertaken as part of both the CROSS and CUPID R&D programs.

210 2 Detector construction and operation

211 2.1 $\text{Li}_2^{100}\text{MoO}_4$ scintillating bolometer fabrication

212 We construct a dual-readout cryogenic particle detector from a primary scintillating absorber and
213 a light detector. The $\text{Li}_2^{100}\text{MoO}_4$ absorber consists of a $45\times 45\times 45$ mm crystal ($\sim 98\%$ enrichment
214 in ^{100}Mo) of mass 279.42 g. We randomly chose the sample from the batch of 32 identical crystals.
215 The crystals were grown starting from purified ^{100}Mo powder and using the low-temperature-
216 gradient technique at the Nikolaev Institute of Inorganic Chemistry (Novosibirsk, Russia). The
217 $\text{Li}_2^{100}\text{MoO}_4$ samples are not perfectly cubic-shaped¹ due to not optimal growing conditions (in
218 particular, the platinum crucible size was not large enough), adapted for the growth of up to
219 $\varnothing 50$ mm crystal boules [? ? ?]. A Neutron Transmutation Doped (NTD) Ge thermistor [?] with a
220 size of $3\times 3\times 1$ mm and a P-doped Si chip [?] were epoxy-glued on the crystal top. The dependency
221 of the NTD Ge resistance on temperature can be approximated as $R(T) = R_0 \cdot e^{(T_0/T)^{0.5}}$ with the
222 parameters $T_0 \sim 3.8$ K and $R_0 \sim 1.5 \Omega$. The Si chip is used as a resistive element to periodically
223 inject constant energy pulses used for off-line stabilization of the bolometric response [?]. The
224 crystal holder is made from copper to host cubic crystals of up to 5 cm side and optical bolometers
225 at their top and/or bottom [? ? ?]. As for the light detector (LD) we use a SiO-coated Ge wafer
226 of 44 mm diameter and 0.175 mm thickness, instrumented with a $3\times 1\times 1$ mm NTD. The LD was
227 mounted in the copper holder near the $\text{Li}_2^{100}\text{MoO}_4$ detector (LMO).

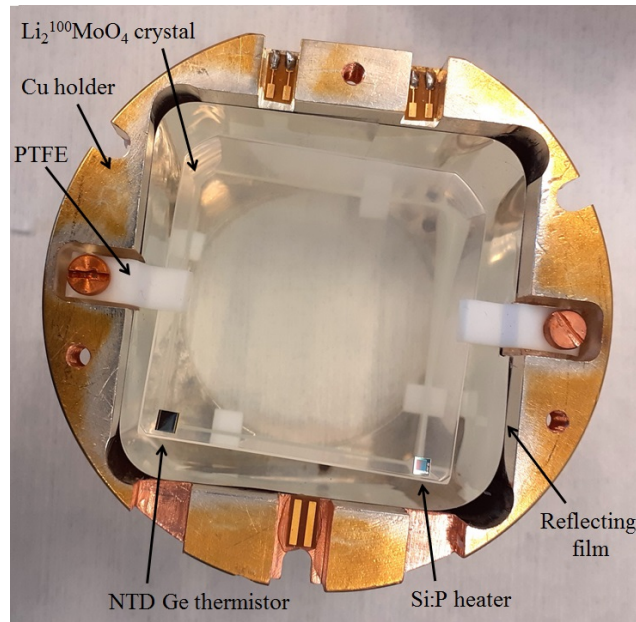


Figure 1. A photograph of the partially assembled $\text{Li}_2^{100}\text{MoO}_4$ scintillating bolometer; the construction elements (see text) are labeled. A $\varnothing 45$ mm hole at the bottom of the holder, visible in transparency, acts as an entrance window for the $\text{Li}_2^{100}\text{MoO}_4$ scintillation light to be registered by a bolometric Ge light detector.

228 The crystal is fixed inside the copper holder by PTFE (polytetrafluoroethylene) pieces, as
229 seen in Fig. 1. The PTFE supports act also as thermal contacts to the heat sink of the cryostat.

¹There are edge chamfers on the crystals, see Fig. 1.

230 The Cu holder of the detector is coated with Au to avoid oxidation, while the internal part of the
231 holder is also coated with Ag to improve light reflection. The $\text{Li}_2^{100}\text{MoO}_4$ crystal inside the Cu
232 housing is surrounded with a Vikuiti™ reflecting film, which is the same used in LUMINEU and
233 CUPID-Mo. The NTD Ge is wire-bonded with Au wires, while the heater is bonded with Al wires.
234 A $^{238}\text{U}/^{234}\text{U}$ source is placed on the holder's top cap. The source was obtained by depositing
235 an uranium-containing liquid drop on a thin copper substrate that was then dried by evaporation.
236 Part of the alpha particles (as well as nuclear recoils) emitted are degraded in energy. The LD is
237 fabricated in the same way using a dedicated Cu holder, three PTFE elements, and an NTD Ge
238 sensor glued. A ^{55}Fe X-ray source is placed close to the LD to irradiate the Ge surface opposite to
239 the $\text{Li}_2^{100}\text{MoO}_4$ absorber.

240 **2.2 Low-temperature underground measurements**

241 We tested the detector in the CROSS Cryogenic Underground (C2U) facility [?], in operation at
242 the Canfranc laboratory (Spain) since April 2019. The cryostat is placed inside a Faraday cage
243 with acoustic isolation, formerly used by the ROSEBUD dark matter experiment [?]. The set-up
244 operates a pulse-tube (Cryomech PT415) based dilution refrigerator, developed by CryoConcept
245 (France), which is also assisted by Ultra Quiet Technology™ (UQT) to mitigate vibrations [?].
246 During the cryostat commissioning, it was found the UQT to efficiently reduce vibrations in the
247 vertical direction, but not as much horizontally [?] resulting in a noise excess affecting the
248 bolometric performance [?]. Thus, the hybrid bolometer was spring-suspended from the detector
249 plate. In order to reduce the environmental background, the cryostat is surrounded externally by
250 a 25 cm thick low-radioactivity lead shield. Moreover, the detector volume inside the cryostat is
251 shielded from the dilution unit and cryostat upper parts with a 13 cm thick disk made of sandwiched
252 lead and copper (120 kg total mass). The shielding of the set-up has not been completed yet, in
253 particular an anti-radon Plexiglas box (to be flushed with a deradonized air) and a muon veto will
254 be installed soon.

255 The signal readout is based on a low-noise room-temperature DC front-end electronics [?]
256 tracing back to the Cuoricino experiment. The data acquisition (DAQ) is a new design candidate for
257 CUPID [?] and consists of two 12-channel boards with a programmable 6-pole Bessel-Thomson
258 anti-aliasing filter and integrated 24-bit ADC. A cut-off frequency of the low-pass filter can be set
259 from 24 Hz up to 2.5 kHz. With the 24 bit ADC resolution, the input noise is not limited by the
260 ADC even with the lowest gain value set at a programmable-gain amplifier (PGA). An additional
261 advantage of such ADC resolution is that the PGA stage can be made much simpler or removed,
262 with less power consumption, cost, and space. The sampling rate up to 25 kS/s can be set (250 kS/s
263 with half of channels). The ADC-digitized continuous data are readout by an external FPGA (field-
264 programmable gate array) module and then transferred to a personal computer via Ethernet. The
265 DAQ control is done with the help of a MATLAB-based graphical user interface program. The
266 monitoring on-line of the data quality is realized as a LabVIEW application.

267 We collected data from the end of December 2019 until the beginning of April 2020. The
268 measurements were performed at temperatures 18 and 12 mK. We periodically calibrated the LMO
269 by inserting a thoriated tungsten wire inside the lead shield. We chose the working points for
270 both operational temperatures to be a few nA current on the NTD sensor resulting in a few M Ω
271 resistance. The data are sampled continuously at a 2 kS/s sampling rate, and the full data stream is

Table 1. Performance of a scintillating bolometer based on the $\varnothing 44$ mm Ge light detector coupled to the 45 mm side $\text{Li}_2^{100}\text{MoO}_4$ cubic-shaped scintillator. We report the detectors rise and decay times, the signal amplitude per unit of deposited energy, the energy resolution (FWHM) of the baseline after the optimum filter, at 5.9 keV X-ray of ^{55}Mn (LD), and at 2615 keV γ quanta of ^{208}Tl (LMO). We skip the computation of FWHM at 2615 keV for the 18 mK dataset due to poor statistics of the γ peak. Particle identification parameters (defined in Sec. 3.2) as light yield for $\gamma(\beta)$ s $LY_{\gamma(\beta)}$ and a quenching factor for α particles QF_{α} , as well as the discrimination power between α and $\gamma(\beta)$ distributions $DP_{\alpha/\gamma(\beta)}$ for events selected in the 2.0–5.1 MeV energy range are also quoted.

Channel	Parameter	18 mK	12 mK
LD	Rise time (ms)	1.7	2.8
	Decay time (ms)	9.2	8.6
	Signal ($\mu\text{V}/\text{keV}$)	1.20	1.44
	FWHM (keV) at baseline	0.300(1)	0.210(1)
	FWHM (keV) at 5.9 keV X-ray	0.282(5)	0.315(4)
LMO	Rise time (ms)	18	25
	Decay time (ms)	150	160
	Signal ($\mu\text{V}/\text{keV}$)	0.017	0.036
	FWHM (keV) at baseline	4.2(2)	2.5(1)
	FWHM (keV) at 2615 keV γ	–	6.0(5)
LMO	$LY_{\gamma(\beta)}$ (keV/MeV)	0.635(2)	0.638(1)
& LD	QF_{α} (^{210}Po)	0.192(1)	0.199(4)
	$DP_{\alpha/\gamma(\beta)}$	7.4(4)	7.9(1)

272 written to disk for offline analysis. The Bessel-Thomson cut-off frequency was set at 300 Hz, as a
 273 compromise between the bandwidth of the LMO (slow) and LD (relatively fast).

274 We used around-3-week-long stable periods of data for the analysis at each regulated temper-
 275 ature, not affected by external events (e.g. power cuts). We select 314 h of physics data at each
 276 temperature and 65 and 220 h of the ^{232}Th calibration data at 18 and 12 mK, respectively.

277 The acquired data are triggered offline to tag discrete energy depositions. The triggered pulses
 278 are then processed by the optimum filter technique [?] to evaluate the signal amplitude (i.e. energy)
 279 and several pulse-shape parameters. In the reconstruction of the coincidences between the LMO
 280 and LD, we account for the LD faster response and correct for its constant time shift with respect to
 281 the LMO signal, similarly to the method described in [?].

282 3 Results

283 3.1 Detector performance

284 The performance parameters achieved by the LMO and LD in the 18 and 12 mK tests are listed in
 285 Table 1. The rise and decay time constants, defined respectively as time intervals of the (10–90)%
 286 rising edge and (90–30)% trailing edge relative to the signal maximum, of the LMO are ~ 0.02 and

287 ~ 0.15 s, respectively. We expect the LD response to be faster by an order of magnitude because
 288 of the smaller heat capacity of both the Ge absorber and the NTD thermistor. The time constants
 289 obtained are in agreement with the results of previous investigations of similar size LMOs and LDs
 290 [? ?]. It is worth noting that the time response of the bolometric detectors depend on the operation
 291 temperature and the sensor polarization (see, e.g., [?]). However, optimization of the detector time
 292 response² was out of the scope of the present study.

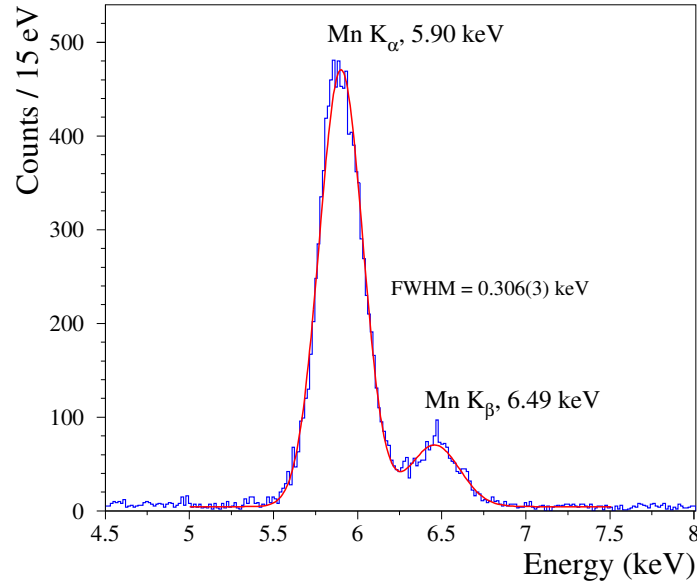


Figure 2. The energy spectrum of the ⁵⁵Fe X-ray source measured by a 1.4 g Ge bolometric light detector over 913 h (12 and 18 mK data) in the CROSS pulse tube based cryogenic facility at the Canfranc underground laboratory (Spain). A fit to the data by a model assuming a double-Gaussian function and a flat background component is shown by solid (red) line. The energy resolution (FWHM) is quoted for the 5.9 keV X-ray peak of Mn K_α.

293 The LD signal amplitude per unit of deposited energy is $1.2 \mu\text{V}/\text{keV}$ at 18 mK and $1.4 \mu\text{V}/\text{keV}$
 294 at 12 mK. The LMO signal amplitude is of course inferior, $17 \text{ nV}/\text{keV}$ at 18 mK and doubles at
 295 12 mK. Since the working points were not optimized to get the highest sensitivity, these results are
 296 good but not extraordinary among similar devices [? ?].

297 The LD is calibrated with the 5.9 and 6.5 keV X-rays emitted by the ⁵⁵Fe source. The energy
 298 spectrum of the ⁵⁵Fe source gathered over 913 h of physics and thorium calibration runs is shown
 299 in Fig. 2. The almost fully resolved Mn K_α/K_β doublet is visible thanks to the high LD energy
 300 resolution: ≈ 0.3 keV FWHM at 5.9 keV. The baseline noise is 0.2–0.3 keV FWHM, demonstrating
 301 a reasonably low threshold. It is worth noting that such devices do not always show a high energy
 302 resolution even if characterized by ten(s) eV RMS noise³, due to the position-dependent response

²In particular, to get the fastest response in view of the rejection of random coincidence events induced background in the ¹⁰⁰Mo $0\nu 2\beta$ region of interest [? ? ?].

³For example, the Mn doublet resolution of 0.3–0.5 keV FWHM was measured with LDs made of 30–45 μm thick Ge wafers [?], while the 0.08 keV FWHM resolution was achieved by a 33 g Ge bolometer ($\varnothing 20 \times 20$ mm) characterized by a similar noise level [?].

303 of thin bolometers.

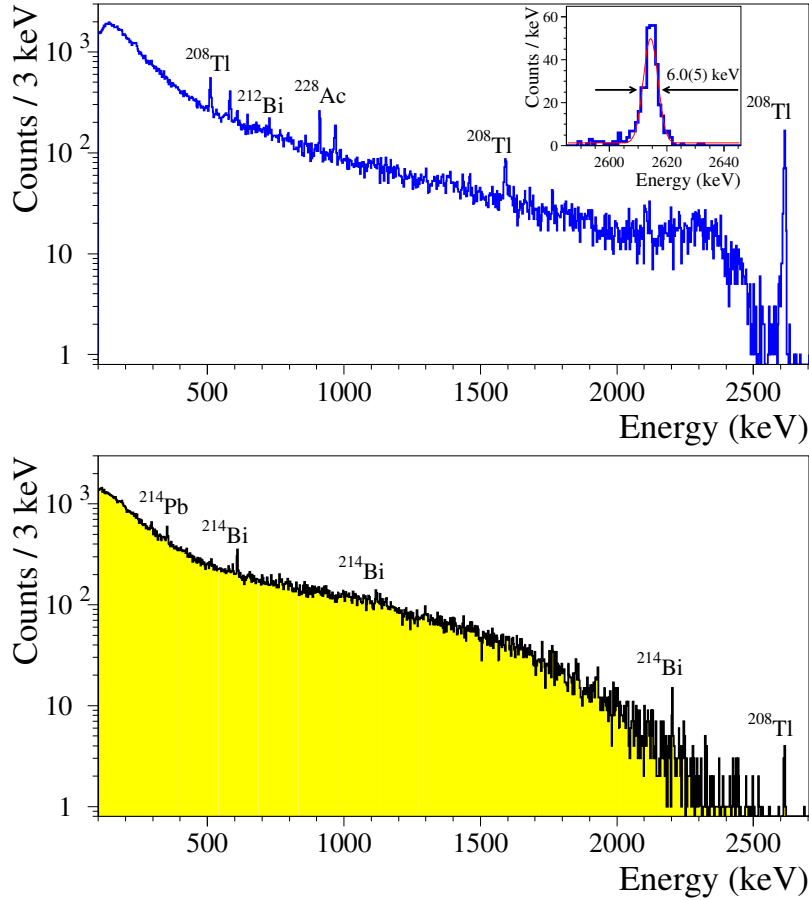


Figure 3. The energy spectra of $\gamma(\beta)$ events accumulated by the LMO over the calibration (285 h; top panel) and physics data (628 h; bottom panel) measurements in the C2U facility at the Canfranc underground laboratory. The most prominent γ peaks are labeled. The contribution of α events to the physics data has been removed with the scintillation light based particle identification (see text). The inset shows the γ peak with energy of 2615 keV in the calibration data together with a fit and the calculated energy resolution (FWHM).

304 We measured the LMO energy scale and resolution with the most intense gamma peaks in the
 305 thorium spectrum, illustrated in Fig. 3 (top panel). Because of the incomplete shielding, the physics
 306 data (Fig. 3, bottom panel) also exhibit several γ peaks from residual environmental radioactivity
 307 (daughters of ^{226}Ra and ^{228}Th sub-chains). The $^{238}\text{U}/^{234}\text{U}$ alpha source also emits β particles
 308 from ^{234m}Pa decays ($Q_\beta = 2.27$ MeV [?]), which, together with the ^{100}Mo $2\nu 2\beta$ decays [?], are
 309 responsible for the most part of the continuum background above 0.5 MeV, seen in Fig. 3 (bottom
 310 panel).

311 The energy dependence of the LMO energy resolution is presented in Fig. 4. The results
 312 extracted from physics data are limited by the poor statistics. The detector demonstrates a good
 313 energy resolution in a wide energy interval exhibiting a peak width slightly increasing with energy,
 314 in agreement with early findings [? ?]. In particular, we achieved a 6 keV energy resolution
 315 (FWHM) for γ -ray quanta of ^{208}Tl with energy 2615 keV, and a 2.5 keV FWHM baseline noise.

316 The resolution at the $Q_{2\beta}$ of ^{100}Mo is expected to be very similar (Fig. 4). These results are
 317 in agreement with prior measurements for cylindrical LMOs [? ? ?], confirming an excellent
 318 bolometric performance independent of the crystal shape. It is also evident that a low baseline noise
 319 is crucial in obtaining a high energy resolution with a $\text{Li}_2^{100}\text{MoO}_4$ bolometer. It is worth noting,
 320 the lowest noise achieved with the LMO is a factor 2–4 worse than the best reported values for
 321 large-volume lithium molybdate bolometers [? ?]. Thus, taking into account sub-optimal noise
 322 level of the present study, there is still room for improvement.

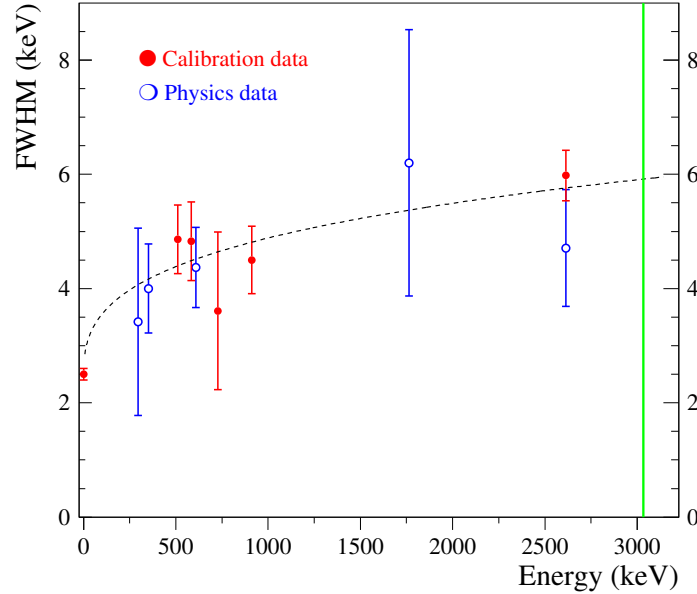


Figure 4. Energy dependence of the 279 g $\text{Li}_2^{100}\text{MoO}_4$ bolometer energy resolution (FWHM) measured in the calibration (filled circles; 12 mK) and physics (open circles; 18 and 12 mK) runs. The fitting curve is shown by the dashed line, while the solid line indicates the ^{100}Mo $Q_{2\beta}$.

323 3.2 Particle identification capability

324 Coincidences between the LMO and LD have been used to probe the scintillation based particle
 325 identification (PID). For each event triggered by the LMO we calculated a PID parameter, the so-
 326 called light yield (LY), defined as the ratio of the LD to LMO measured energy. The LY dependence
 327 on particle energy is shown in Fig. 5, where the population of $\gamma(\beta)$ events is clearly separated from
 328 α 's. Such a powerful separation is achieved thanks to the quenching of the scintillation light for α
 329 particles with respect to $\gamma(\beta)$'s of the same energy and low noise of the LD. Different ionization
 330 properties lead also to a different amplitude measured by the LMO. Figure 5 shows a $\sim 7\%$ increase
 331 of an α event energy with respect to the gamma energy scale, in agreement with previous studies of
 332 LMO bolometers [? ?]. This difference, called thermal quenching, hints at a possibility of PID by
 333 pulse-shape analysis of the heat channel itself [?], but it is by far less reproducible due to a strong
 334 dependence on the noise conditions⁴.

⁴Since the present detector does not have the CROSS technology of the surface coating for PID purpose, we skip an analysis of pulse-shape discrimination of α events.

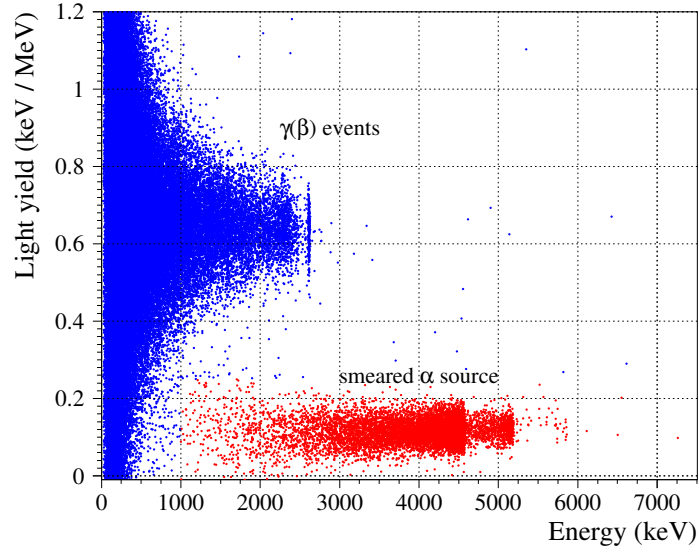


Figure 5. Light yield as a function of energy deposited in the LMO and measured in a 125 h long ^{232}Th calibration at 12 mK. The energy scale is calibrated with γ quanta. The population of $\gamma(\beta)$ events is clearly separated from the α events, mainly originated by the $^{238}\text{U}/^{234}\text{U}$ smeared α source. The α events shown in red were selected above 1 MeV with a LY cut below 0.25 keV/MeV.

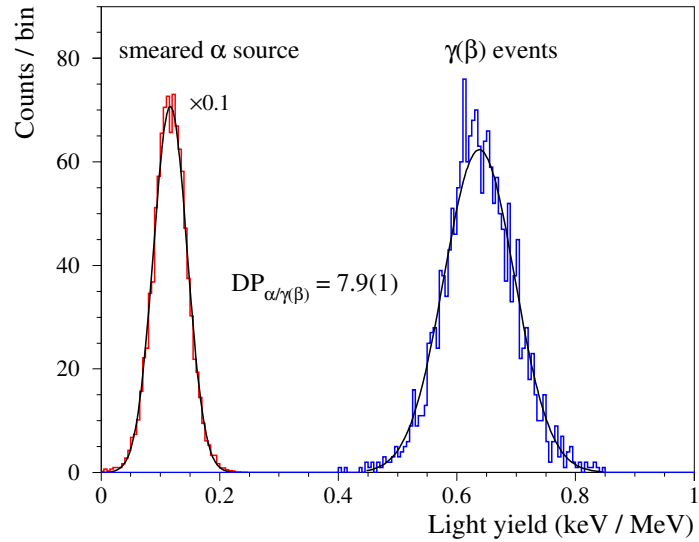


Figure 6. The light yield distributions for α and $\gamma(\beta)$ particles, selected in the 2.0–5.1 MeV energy interval. The former distribution is rescaled by a factor 0.1 to improve the visibility of the later one. A Gaussian fit to each distribution is shown by a solid line. The discrimination power between the two populations is ~ 8 .

335 In order to investigate a LY -based $\alpha/\gamma(\beta)$ separation close to the ^{100}Mo $0\nu 2\beta$ region of interest
 336 (ROI), we selected events within the 2.0–5.1 MeV energy range and a LY interval of 0.4–1.0
 337 keV/MeV for $\gamma(\beta)$'s and 0–0.25 keV/MeV for α 's; both are shown in Fig. 6. A Gaussian fit to each
 338 distribution provides a LY mean value (μ) and standard deviation (σ), which we used to calculate
 339 the so-called discrimination power defined as

$$DP_{\alpha/\gamma(\beta)} = |\mu_{\gamma(\beta)} - \mu_{\alpha}| / \sqrt{\sigma_{\gamma(\beta)}^2 + \sigma_{\alpha}^2}. \quad (3.1)$$

340 The $DP_{\alpha/\gamma(\beta)}$ based on the present data is around 8 (Table 1), meaning about $8\sigma_{\alpha}$ of alpha event
 341 rejection while keeping almost 100% of $\gamma(\beta)$'s. This rejection power fully satisfies the CUPID goal
 342 of identifying 99.9% of alpha particles (corresponding to $DP_{\alpha/\gamma(\beta)} \sim 3.1$).

343 The LMO light yield for $\gamma(\beta)$ events ($LY_{\gamma(\beta)}$) was found to be 0.64 keV/MeV, similar to one
 344 measured with cylindrical shaped LMOs of $\varnothing 44 \times 45$ mm size [? ? ?]. However, in the present
 345 study the light collection efficiency was affected by the smaller area of the LD (15 cm^2) with respect
 346 to the LMO surface facing it (20 cm^2) and by the entrance window of the Cu holder ($\varnothing 45$ mm).
 347 Thus, considering only the direct light, the $LY_{\gamma(\beta)}$ is expected to be ~ 0.85 keV/MeV, once a 45 mm
 348 side square LD is coupled to the LMO. In case of the use of two LDs, the LY should be roughly
 349 doubled, as demonstrated by CUPID-Mo [? ?]. The quenching factor (QF_{α}) for α particles of
 350 ^{210}Po observed in the data (see the next section) is 0.2⁵, in agreement with the previous data [? ?
 351 ?].

352 3.3 $\text{Li}_2^{100}\text{MoO}_4$ crystal radiopurity

353 A highly-efficient PID together with a good energy resolution of the LMO operated over four
 354 weeks of background measurements allow us to quantify the $\text{Li}_2^{100}\text{MoO}_4$ radiopurity with a high
 355 sensitivity. The spectrum of alpha events selected from the physics data (and recalibrated to α
 356 energy) is presented in Fig. 7; the energy interval covers most Q_{α} -values of radionuclides from the
 357 U/Th chains. As it is seen in Fig. 7, the use of the $^{238}\text{U}/^{234}\text{U}$ smeared α source prevents estimation
 358 of the alpha activity of ^{232}Th , ^{238}U and some of the daughters with $Q_{\alpha} \leq 4.8$ MeV. However, we can
 359 investigate a possible contamination by ^{226}Ra and ^{228}Th , which are the most harmful contaminants
 360 for $0\nu 2\beta$ searches.

361 The energy region above 4.8 MeV contains only two peak-like structures both ascribed to ^{210}Po
 362 α events, and originated by the ^{210}Pb contamination [?]. A clear peak at 5.4 MeV is induced by the
 363 ^{210}Po decays in the $\text{Li}_2^{100}\text{MoO}_4$ crystal bulk with the activity of 80(12) $\mu\text{Bq/kg}$. A ^{210}Po (^{210}Pb)
 364 bulk contamination on the level of ten(s)–hundred(s) $\mu\text{Bq/kg}$ is typical for $\text{Li}_2^{100}\text{MoO}_4$ crystals [?
 365 ? ? ?]. A broad distribution peaked at 5.3 MeV is caused by the ^{210}Po decay on the surface of
 366 materials facing the LMO (a 0.1 MeV energy is taken away by the ^{206}Pb nuclear recoil). The decays
 367 of ^{210}Po at surfaces of the detector materials can populate the ^{100}Mo $0\nu 2\beta$ ROI as energy-degraded
 368 alpha events, but they can be easily rejected thanks to the efficient PID of $\text{Li}_2^{100}\text{MoO}_4$ scintillating
 369 bolometers. Also, the total rate of ^{210}Po events (~ 0.06 mHz) is rather low to be a notable source of
 370 pile-ups, which are of certain concern for slow response thermal detectors [?].

⁵Such a parameter is typically quoted without the correction from the thermal quenching and we follow that convention here.

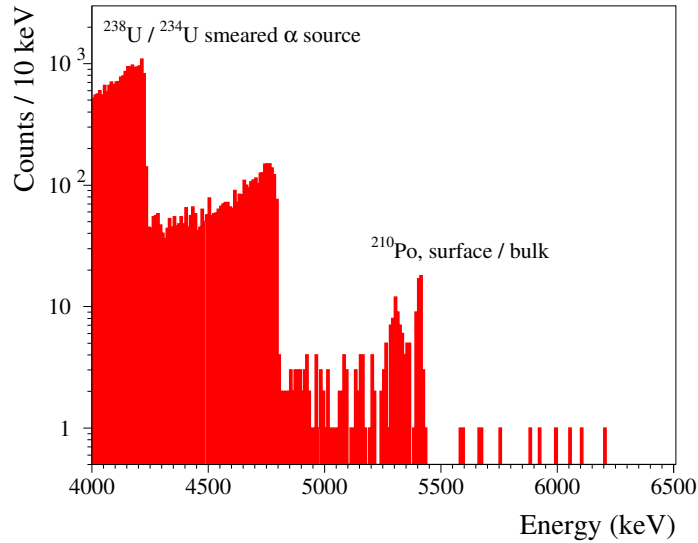


Figure 7. A part of the α energy spectrum accumulated by the LMO operated over 628 h in the CROSS underground cryostat in Canfranc. The energy interval covers the Q_α -values of the most α -active radionuclides from U/Th decay chains. In addition to a dominant contribution from the used $^{238}\text{U}/^{234}\text{U}$ source, the spectrum exhibits only two populations of ^{210}Po originated by external (surface of nearby materials) or internal (crystal bulk) contaminations of the detector.

371 The spectrum shows no other structures, so we can only set limits on other radionuclide
 372 contaminations. In order to be conservative, we considered all events within 25 keV of each
 373 expected peak location. The background (1 count per 50 keV) was estimated in the 5.65–5.75 and
 374 5.85–5.95 MeV energy intervals, containing no Q_α -value of U/Th radionuclides. The data exhibit
 375 no events of ^{228}Th ($Q_\alpha = 5520$ keV [?]) and two counts of ^{222}Rn ($Q_\alpha = 5590$ keV [?]; a daughter
 376 of ^{226}Ra), thus we place 90 confidence level (C.L.) upper limits of 1.6 and 4.9 counts, respectively
 377 [?]. A selection efficiency of 95.7% was estimated using alpha events of the $^{238}\text{U}/^{234}\text{U}$ smeared α
 378 source, distributed in the 3.5–4.8 MeV energy interval. Therefore, the activity of ^{228}Th and ^{226}Ra
 379 in the $\text{Li}_2^{100}\text{MoO}_4$ crystal bulk is below 3 and 8 $\mu\text{Bq/kg}$ at 90% C.L., respectively. Taking into
 380 account the reasonably short half-lives of ^{228}Ra (5.75 yr [?]) and ^{228}Th (1.91 yr [?]), the limit on
 381 the ^{228}Th activity can also represent the ^{232}Th contamination in the crystals, as e.g. seen in [? ? ?
 382].

383 The limits on the ^{228}Th and ^{226}Ra activity in the studied $\text{Li}_2^{100}\text{MoO}_4$ crystal are on the same
 384 level as reported by LUMINEU [? ?], which were obtained by the analysis of a comparable
 385 exposure. A significantly larger exposure of the CUPID-Mo experiment [? ? ?] shows that the
 386 level of remaining contaminants in $\text{Li}_2^{100}\text{MoO}_4$ scintillators can be even an order of magnitude
 387 lower. As the protocol of the CROSS crystal production was the one adopted by LUMINEU and
 388 CUPID-Mo, it seems natural to assume the radiopurity of the CROSS crystals to be similar to that
 389 of CUPID-Mo ones. It is worth noting that the ^{228}Th (^{232}Th) and ^{226}Ra contamination on the level
 390 of 10 $\mu\text{Bq/kg}$ is compatible with a background contribution below 10^{-4} counts/yr/kg/keV to the
 391 ^{100}Mo $0\nu 2\beta$ ROI, and it is fully acceptable not only for the medium-scale CROSS experiment (with
 392 ~ 10 kg detector mass), but also for the tonne-scale extension of CUPID.

393 4 Conclusions

394 We report that performance and radiopurity of a scintillating bolometer based on a large cubic-
395 shaped $\text{Li}_2^{100}\text{MoO}_4$ crystal —randomly taken from 32 identical crystals (with a 45 mm side and
396 a mass of 0.28 kg each) of the CROSS $0\nu 2\beta$ project— are similar to those of cylindrical 0.2 kg
397 $\text{Li}_2^{100}\text{MoO}_4$ bolometers, used in LUMINEU and CUPID-Mo 2β experiments. In particular, the
398 $\text{Li}_2^{100}\text{MoO}_4$ detector energy resolution at 2615 keV γ quanta (as well as its approximation to
399 3034 keV, the ^{100}Mo 2β decay energy) is 6 keV FWHM. A scintillation light yield of the cubic-
400 shaped crystal, 0.64 keV/MeV for $\gamma(\beta)$'s, is compatible to that of cylindrical crystals. However,
401 the measured light yield is affected by about 30% lower detection surface of the optical bolometer
402 with respect to the nearby $\text{Li}_2^{100}\text{MoO}_4$ crystal face. In spite of sub-optimal light collection, a full
403 separation ($\sim 8\sigma$) between α and $\gamma(\beta)$ events above 2 MeV has been achieved. A high radiopurity
404 of the cubic-shaped $\text{Li}_2^{100}\text{MoO}_4$ crystal was also demonstrated by the present study, where only
405 ^{210}Po is detected with the activity of 80(12) $\mu\text{Bq/kg}$, while the content of ^{228}Th and ^{226}Ra (the most
406 harmful radionuclides from U/Th families for $0\nu 2\beta$ searches) is estimated to be less than 3 and
407 8 $\mu\text{Bq/kg}$, respectively.

408 The performed investigation additionally proves the excellent prospects of $\text{Li}_2^{100}\text{MoO}_4$ scin-
409 tillating bolometers for high-sensitivity $0\nu 2\beta$ decay searches. The cubic shape of large-volume
410 ($\sim 90 \text{ cm}^3$) $\text{Li}_2^{100}\text{MoO}_4$ crystals allows a more compact detector array structure and thus the de-
411 ployment of a larger isotope mass in the experimental volume, as well as an increased efficiency
412 of multi-site event detection. In view of these results, large-mass ($\sim 0.3 \text{ kg}$) radiopure cubic-
413 shaped $\text{Li}_2^{100}\text{MoO}_4$ crystals operated as bolometers satisfy the demands of the CROSS and CUPID
414 projects.

415 Acknowledgments

416 The CROSS and CUPID Collaborations thank the directors and staff of the Laboratorio Subterráneo
417 de Canfranc and the technical staff of our laboratories. This work was supported by the Istituto
418 Nazionale di Fisica Nucleare (INFN); by the European Research Council (ERC) under the European
419 Union Horizon 2020 program (H2020/2014-2020) with the ERC Advanced Grant no. 742345 (ERC-
420 2016-ADG, project CROSS) and the Marie Skłodowska-Curie Grant Agreement No. 754496; by the
421 Italian Ministry of University and Research (MIUR) through the grant Progetti di ricerca di Rilevante
422 Interesse Nazionale (PRIN 2017, grant no. 2017FJZMCJ); by the US National Science Foundation
423 under Grant Nos. NSF-PHY-1614611 and NSF-PHY-1401832; by the P2IO LabEx (ANR-10-
424 LABX-0038) managed by the Agence Nationale de la Recherche (France). This material is also
425 based upon work supported by the US Department of Energy (DOE) Office of Science under Contract
426 Nos. DE-AC02-05CH11231 and DE-AC02-06CH11357; and by the DOE Office of Science, Office
427 of Nuclear Physics under Contract Nos. DE-FG02-08ER41551, DE-SC0011091, DE-SC0012654,
428 DE-SC0019316, DE-SC0019368, and DE-SC0020423. This work was also supported by the
429 Russian Science Foundation under grant No. 18-12-00003 and the National Research Foundation
430 of Ukraine under Grant No. 2020.02/0011.